Title

Dynamics of tilted eddies in a transversal flow at the edge of tokamak plasmas and the consequences for L–H transition

Journal

Plasma Physics and Controlled Fusion, 55(12)

ISSN

0741-3335

Authors

Fedorczak, N
Ghendrih, Ph
Hennequin, P
et al.

Publication Date

2013-12-01

DOI

10.1088/0741-3335/55/12/124024

Peer reviewed

Dynamics of tilted eddies in a transversal flow at the edge of tokamak plasmas and consequences for L-H transition

N. Fedorczak and Ph. Ghendrih

*CEA, IRFM, F-13108 Saint-Paul-Lez-Durance, France**

P. Hennequin

Laboratoire de Physique des Plasmas, Ecole Polytechnique,

CNRS, 91128 Palaiseau Cedex, France

G.R. Tynan and P.H. Diamond

Center for Momentum Transport and Flow Organization,

University of California at San Diego, San Diego, California 92093, USA

P. Manz

Max-Planck-Institut für Plasmaphysik Boltzmannstrasse 2,D-85748, Garching, Germany

Abstract

The dynamical interaction between eddies and shear flow is investigated through a simplified model of vorticity conservation with tilted eddies. Energy is transfered either to the flow or to eddies, depending on the eddy tilt with respect to the flow shear. When eddies are tilted in the shear direction, the system is favorable to shear increase: tilt instability or negative viscosity phenomenon. When eddies are tilted in the opposite direction, the shear flow is damped via a Kelvin-Helmholtz process. The tilt instability generally dominates the interaction on the largest radial scale, but a fraction of the energy cascades to smaller radial scales through the alternation of tilting and Kelvin-Helmholtz dynamics. Within this eddy description, we show that the symmetry breaking required to generate a net residual stress is set by the intrinsic eddy tilt. We recall that magnetic shear can provide an intrinsic tilt to ballooning modes at the edge of tokamak plasmas, with an orientation which depends on flux surface geometry. In L-mode weak shear regimes, this residual stress can dominate the Reynolds stress. Coupled to momentum sources acting in the scrape-off layer, it can induce a significant difference of edge radial electric field between lower single null and upper single null geometries. A comparison with experimental profiles measured across the edge of Tore Supra L-mode plasmas is discussed.

* nicolas.fedorczak@cea.fr

I. INTRODUCTION

Rotation impacts confinement in tokamak plasmas: among other effects, toroidal rotation can directly mitigate specific MHD modes which are normally locked to tokamak walls [1], and differential transversal rotation can impact the level of turbulent transport [2]. It is believed to trigger transport barriers in tokamaks, and especially that of the H-mode barrier [3–5]. Underlying concepts are relatively simple, although their interplay can be complex. First, differential flows can break apart turbulent eddies and thus reduce the level of transport across shear layers [6]. Second, turbulence can drive large scale flows via the Reynolds stress [7] which can deplete the turbulence via tilting instabilities [8–10], sometimes referred to as negative viscosity or tilt-stretch-absorption process [11, 12]. On the other hand, a general picture in fluid mechanics is that differential rotation is a source of turbulence via Kelvin-Helmholtz mechanisms [13]. Last but not least, rotation can be spontaneously generated in a system a-priori free of any external torque, by the action of so called *residual stresses* [4], which act to exchange momentum between the system and its surroundings. The physics of spontaneous rotation is investigated for its beneficial impact in a large tokamak like ITER where external torques will be probably too small to avoid MHD instabilities [14], and where onset of transport barriers are mandatory to access the required performance. In most of models, the drive of rotation arises from symmetry breaking in the turbulence properties, either in real or phase space. The flow shear itself breaks the symmetry of turbulent eddies and induces tilting instabilities. Also the geometrical asymmetry of both magnetic flux surfaces and turbulent activity can generate parallel rotation [15–17], or even transverse rotation at the edge [18]. In the latter work the idea was proposed that such a mechanism could be responsible for the definition of favorable and unfavorable plasma geometries with respect to the transverse shearing rate at the plasma edge [19–21].

All these concepts relative to the interaction between transverse flows and turbulence in tokamaks are often treated separately, and rely on mathematical descriptions which are often non-intuitive. Here we summarize an approach of coherent eddies interacting with shear flows based on simplified geometrical properties of these eddies immersed in the flow. Reynolds stress corresponds to tilted potential eddies in real space, and the tilt evolves in the shear flow, while the total energy or enstrophy of the system is conserved. A reference work [22] contains the key points of the derivation of this model, the present work is an extension of it. The model captures the tilting instability or negative viscosity, radial decorrelation of eddies, Kelvin-Helmholtz mechanisms, and residual stresses. In the first section we show that both tilting and Kelvin-Helmholtz instabilities

take place in the dynamical interaction between eddies and shear flows, with a certain hierarchy. The concept of residual stress is treated in the second section, simply as an intrinsic eddy tilt. In a tokamak geometry, an obvious intrinsic tilt originates from the differential magnetic helicity - magnetic shear - as explained in the third section. We explain how poloidal asymmetries of the magnetic flux surfaces are involved, and induce a reorganization of transverse rotation at the plasma edge [18]. In particular, we show in the last section that the transverse flow profile can be strongly impacted by the poloidal position of a single X-point, in agreement with experimental observations.

II. DYNAMICAL INTERACTION BETWEEN TILTED EDDIES AND SHEAR FLOW

We treat the interaction between potential eddies and an electrostatic shear flow in the transverse domain (x, y), taking the magnetic field in the direction z such that x is the radial direction oriented outward and (x, y, z) is orthonormal. The system is assumed uniform along z. The dynamics is described by a generic vorticity conservation equation, voluntary free of sources in order to focus only on the dynamical interaction between potential eddies and a large scale flow (a derivation of this class of equation for magnetized plasma can be found in [23]):

$$\partial_t \omega + v \cdot \nabla \omega = 0 \tag{1}$$

where the vorticity is simply defined as the 2D laplacian of the total space potential Φ: $\omega = \nabla^2 \phi$ and the drift velocity is $v = z \times \nabla \phi$. The above equation is written in normalized units: time is given in ion Larmor periods ω_i^{-1}, distance in hybrid Larmor radius $\rho_S = c_S/\omega_i$ with $c_S^2 = k_B T_e/m_i$, and plasma potential in fraction of electron temperature (T_e given in eV), taken as uniform. All of the interplay and energy transfer between flow and eddies result from the conservation of total vorticity defined as the superposition of eddies and flow vorticity. The radial motion of potential eddies is implicitly canceled by omitting polarization sources from curvature effects [23]. Thus, the model is in principle only valid in a dynamical interval shorter than any interchange growth time.

Without losing generality, the y coordinate can be translated such that the electrostatic flow is null at the position $x = 0$, although in general its gradient is non-zero. Coherent eddies organized along the flux surface $x = 0$ can be locally represented by trigonometric wave vectors (k_x, k_y) and

a radial envelope ϕ_c of width $2\pi/\lambda$ [8, 24]:

$$\phi(t) = \underbrace{\phi_0(t)\cos(\lambda x)}_{\phi_c}\cos(k_x(t)x + k_y y) \tag{2}$$

Note that such a representation is in fact a superposition of 2 waves $(k_x + \lambda, k_y)$ and $(k_x - \lambda, k_y)$ which can interact with a third wave $(2\lambda, 0)$, obviously a vertical flow pattern. Locally ($x \approx 0$), the flow dynamics is simply reduced to the dynamics of its radial gradient, $\partial_x V_y^{flow} = \sigma_S(t)$. Eddy deformation by flow shear [9] is described by a time varying wave vector $k_x(t)$ [25], whereas λ and k_y are assumed constant in time. This assumption is correct in the limit of uniform flow along y, so that k_y is not impacted by vertical compression, and λ is not impacted by radial dilatation.
A physical description of the eddy-flow interaction can be derived. We recall the simplified system of equations ruling the dynamics at $x \approx 0$, as detailed in [22]:

$$\begin{aligned} \partial_t \sigma_S &= -\phi_0^2 \lambda^2 k_x k_y \\ \partial_t \left[\phi_0(\lambda^2 + k_x^2 + k_y^2)\right] &= 0 \\ \partial_t k_x &= -\sigma_S k_y \end{aligned} \tag{3}$$

which describes the flow shear evolution via the source - or Reynolds work- provided by eddies, the eddies amplitude evolution ruled by stretching, and the stretching itself. As shown in [22], the system 3 conserves an enstrophy - or square vorticity [26] - parameter $\kappa_0^2 = \sigma_S^2 + \phi_0^2\lambda^2\left(\lambda^2 + k_y^2 + k_x^2\right)$, which is exchanged between the vertical flow and the chain of eddies. Note however that the system 3 is only a local $x = 0$ approximation of the global dynamics, and its solution depends on the radial modulation pattern fixed as initial conditions. The drive of vertical flow by the Reynolds work, proportional to $-\phi_0^2\lambda^2$ in Eq.3, is in fact proportional to the eddy envelope curvature $\partial_x^2\left(\frac{1}{2}\phi_c^2\right)$ expressed in the trigonometric representation Eq.2. For simplicity, the curvature parameter λ is not allowed to evolve in the system Eq.3, although it changes in time by a mechanism discussed below. With that in mind, the model can describe the main physics of eddy/flow dynamics as rendered by 2D numerical simulations [22], including non linearities.
The previous work [22] was mainly devoted to the application of this system to the tilting instability (TI) in the limit $k_x\sigma_S < 0$, which is the natural orientation of eddies in a shear flow, as described by the third equation of system 3. Multiplying the first equation by σ_S gives the time evolution of the flow enstrophy $\partial_t\sigma_S^2 = -2\phi_0^2\lambda^2 k_y k_x \sigma_S$, which increases in time only if $k_x\sigma_S < 0$ (for a natural eddy envelope $\partial_x^2\left(\frac{1}{2}\phi_c^2\right) < 0$). The condition $k_x\sigma_S < 0$ is defined as a *favorable* eddy tilt with respect to flow amplification. Assuming that eddy amplitude is unchanged during the interaction,

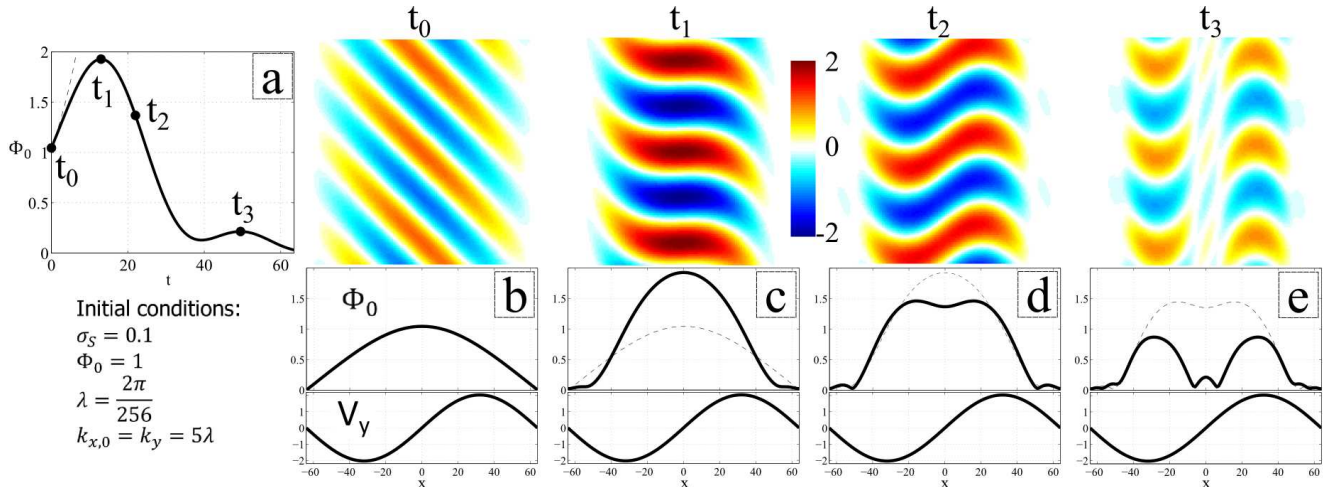

FIG. 1. Numerical simulation of a weak eddy chain in a strong flow shear, with initial conditions set for Kelvin-Helmholtz instability. **a)** Time evolution of the chain amplitude at $x = 0$. The dashed curve represents the linear growth dynamics given by Eq.5. **b)** to **e)** top: 2D eddy structure at different times of the interaction. Bottom: radial profiles of eddy envelope and background flow.

the linear flow dynamics reduces to:

$$\partial_t^2 \sigma_S = \left(\phi_0 \lambda k_y\right)^2 \sigma_S \tag{4}$$

where we identify a flow growth rate $\gamma_\sigma = |\phi_0|\lambda k_y$, proportional to eddies amplitude [8, 9, 24]. In fact the flow cannot grow exponentially for a long period of time since the total enstrophy is conserved: the eddy amplitude decreases and after a certain period of time the flow saturates [22]. This is illustrated by 2D numerical simulations of Eq.1, shown in Fig.1. In this figure the tilting instability starts at time $t = t_1$, for a case of strong shear flow and weak eddies. The gain of enstrophy by the flow is negligible, but eddies are locally depleted around the position $x = 0$. The presence of secondary rebounds and their link with eddy envelope curvature is discussed afterward.

The system shown in Fig.1 is in fact initiated with a reversed TI criterion: $k_x \sigma_S > 0$. This is defined as an *unfavorable* eddy geometry because the Reynolds work damps the flow shear. Since the system 3 conserves enstrophy, the flow damping necessarily implies that the chain is growing in amplitude, which *could* refer to a Kelvin-Helmholtz type of instability (KHI). Assuming a given background shear, the second and third equations in system 3 then give:

$$\partial_t \phi_0 = -\phi_0 \frac{2k_x \partial_t k_x}{\lambda^2 + k_y^2 + k_x^2} = \phi_0 \frac{2k_x k_y \sigma_S}{\lambda^2 + k_y^2 + k_x^2} \tag{5}$$

where we identify the growth rate $\gamma_\phi = \sigma_S \frac{2k_x k_y}{\lambda^2 + k_y^2 + k_x^2}$. This exponential behavior is again misleading, because the radial wave vector evolves in the shear flow and makes the above growth rate decreasing later in time (see initial dynamics in Fig.1a). This rate is positive for the condition $k_x \sigma_S > 0$, which therefore corresponds to a seed eddy chain tilted in opposition to the shear flow. For positive background shear, the maximum initial growth is for $k_x = \sqrt{\lambda^2 + k_y^2}$, which corresponds, in the limit of large radial envelope, to eddies tilted by -45^o.

Now we investigate the non-linear dynamics of this KH configuration. Considering the case of maximum growth, that is for an initial seed chain tilted by $k_{x,0} \approx k_y$, the chain amplitude will effectively grow while the eddy tilt evolves in the shear. If the total enstrophy is dominated by the flow shear, the loss of shear strength is negligible and the tilting evolves as $k_x(t) = k_y - k_y \sigma_S t$. Thus, at the time $t = \frac{1}{\sigma_S}$ (close to time t_1 in Fig.1), the eddy tilt cancels and the Reynolds work vanishes. The flow continues to stretch the eddy into the favorable tilting domain $k_x \sigma_S < 0$, and a TI occurs as pictured earlier. An important remark is that the TI redistributes the enstrophy gained by the eddies during the previous KH, back into the shear flow.

Another KH case is of interest: considering a flow shear initially weak as illustrated in Fig.2, the system will even not reach the state $k_x(t) = 0$, because the shear flow will get totally depleted at an earlier time by the KH process. For initial conditions of tilting $k_{x,0} = \sqrt{\lambda^2 + k_y^2}$ and shear $\sigma_{S,0} > 0$, the KH process will stop when the tilt reaches the value $k_x = k_{x,0}\sqrt{1 - \frac{2\sigma_{S,0}^2}{\kappa_0^2}}$, thus requiring an initial weak shear criterion $\sigma_{S,0}^2 < \frac{1}{2}\kappa_0^2$. In Fig.2, it occurs at $t \approx 400$. At this time the shear flow is null, but eddies manifest a non-zero tilt which gives a Reynolds work according to Eq.3. The flow is then naturally driven into the favorable tilting regime as illustrated in Fig.2 for the time domain $t > 400$. Again, a TI occurs, but here initiated by an initial eddy tilt and not by an initial seed flow. This particular phenomenon introduces the concept of residual stress, which is treated later.

We have described several phenomena which all evolve through a tilting instability pattern: the TI itself, and two cases of initial eddies in the unfavorable tilt regime. As discussed in [22] and mentioned earlier, the tilting instability depletes the chain, locally. This depletion is a priori not impacting the titling criterion $k_x \sigma_S < 0$ since both σ_S and k_x evolve with constant sign. That said, the local depletion implies a modification of the eddy envelope curvature, impacting the Reynolds work in Eq.3: $\partial_t \sigma_S = \partial_x^2 \left(\frac{1}{2}\phi_c^2\right) k_x k_y$. After a finite period of time of TI process, the local eddy curvature reverses sign due to the depletion, and the shear growth stops and reverses.

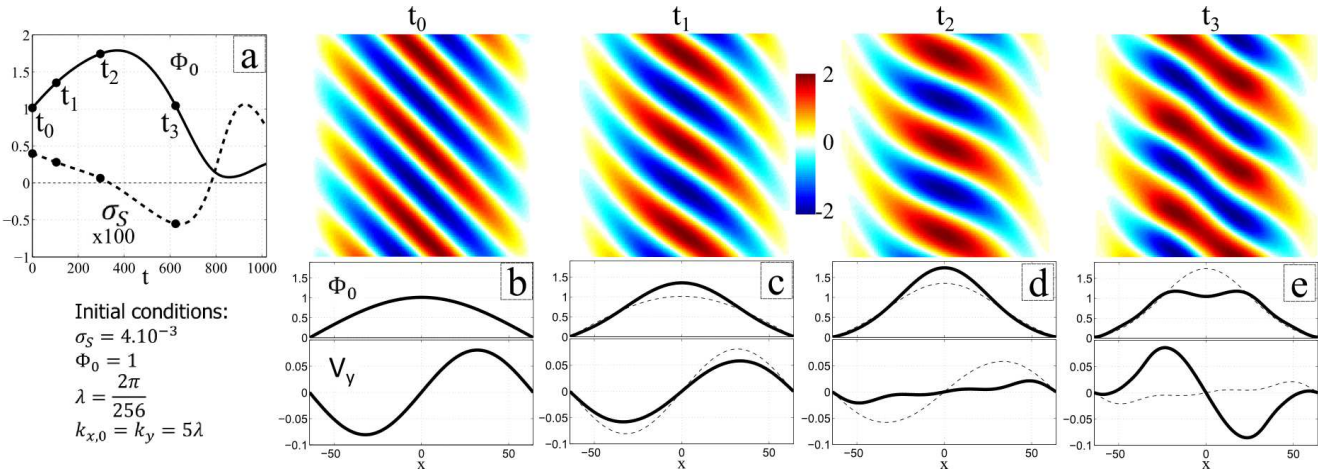

FIG. 2. Numerical simulation of a strong eddy chain in a weak flow shear, with initial conditions set for Kelvin-Helmholtz instability. **a)** Time evolution of the chain amplitude (full curve) and flow shear (dashed) at $x = 0$. **b)** to **e)** top: 2D eddy structure at different times of the interaction. Bottom: radial profiles of eddy envelope and flow.

The chain is locally gaining energy around $x \approx 0$, but with a higher radial modulation than the original one $\lambda_2 > \lambda$. This is a process of Kelvin-Helmholtz type, happening in the time interval $40 < t < t_3$ in Fig.1 and $t > 800$ in Fig.2. After another finite period of time, the local eddy growth induces another reversal in the envelope curvature, and a TI starts again on the radial scale λ_2. As explained in [22], this succession of TI and KHI is indeed observed in laboratory plasmas, on time scales in agreement with the model.

Since the KH takes place on a finer radial scale than the previous TI, the exchange of enstrophy during KH impacts only a fraction of the total space enstrophy, such that the KH cannot balance the shear growth from the previous TI. We can then effectively speak of forward enstrophy cascade in the radial wavenumber space, induced by a coupling between Kelvin-Helmholtz and tilting instabilities. The cascade hierarchy implies that the tilting instability dominates on the largest scale. This conclusion is in agreement with a recent and independent study of shear flow and turbulence interaction by Gürcan in [27]. Also, we come to the same conclusion as expressed by Kim *et al.* in [28], that Kelvin-Helmholtz is not a tertiary instability in the coupling of turbulence and flow. We show indeed that tilting and KH instabilities are concomitant, and that KH play a crucial role in the forward energy cascade, thus in the saturation of the flow drive by TI. Interestingly, the tilting instability is also an inverse enstrophy cascade in the vertical wave space, directed from the small scale eddies to the large scale shear flow. Finally, it is worth mentioning that this mechanism

does not impact the global momentum balance. As illustrated in fig.2, the flow created by the eddies is purely differential and thus its spatial integral vanishes. The reason is that there is no vorticity creation in the process, but only vorticity re-organization.

III. A REPRESENTATION OF RESIDUAL REYNOLDS STRESS

In the previous section we have mentioned an interesting set of initial conditions: no shear flow, but a finite Reynolds work $\Phi_0^2\lambda^2 k_y k_x$ arising from a finite eddy tilt. Naturally, such initial system evolves into a finite shear flow, with the orientation satisfying the TI criterion $\sigma_S k_x < 0$. Thus, an initial k_x in the eddy structure provides a seed for the shear flow: by definition, it is called a residual stress, because a stress exists that is not proportional to the flow nor its gradient. Here, this general concept appears simply as the manifestation of a natural tilt of the eddy chain. Note that, absent any additional physical effects such as a no-slip boundary condition (which could arise from e.g. interactions with a fixed background neutral gas located in the boundary region) such residual stress is not a source of global vorticity, but only provides a mechanism to re-organize the existing vorticity pattern. Let us consider a case where a chain orientation evolves from a reference value $k_{x,0}$ in the background shear σ_S. Across an eddy residence or life time τ, the eddy orientation is about $k_x(\tau) \approx k_{x,0} - k_y\sigma_S\tau$. The Reynolds stress term in the flow dynamics then reads:

$$\begin{aligned} \langle \tilde{v}_r \tilde{v}_y \rangle &\approx -\left\langle \tilde{\phi}^2 k_x k_y \right\rangle \\ &\approx -\left\langle \tilde{\phi}^2 k_y^2 \left[-\sigma_S\tau + \tfrac{k_{x,0}}{k_y} \right] \right\rangle \\ &\approx +\langle v_x^2 \rangle \tau\sigma_S - \langle v_x^2 \rangle \tfrac{k_{x,0}}{k_y} \end{aligned} \tag{6}$$

Understood as a radial flux of poloidal momentum, the first RHS term has a viscous nature because proportional to the gradient of poloidal momentum. It is in fact a negative viscosity term, intrinsically associated to the tilting instability. The second RHS term is the contribution from the initial eddy tilt, proportional to the initial radial wave component. Now we can introduce the concept of favorable and unfavorable residual stress: when the initial tilt satisfies $k_{x,0}\sigma_S < 0$ the residual stress adds to the negative viscosity and is said to be *favorable*. On the other hand, when $k_{x,0}\sigma_S > 0$ the residual stress competes with the negative viscosity and is said to be *unfavorable*. Obviously, the system illustrated in Fig.1&2 start in the unfavorable regime: the initial stress competes with the flow shear. In the second case, it even dominates the negative viscosity and reverses the flow direction. Note that previously, we referred to a process which *could* be of Kelvin-Helmholtz type, although it is in fact the action of an unfavorable residual stress. Looking at this

initial interaction with residual tilt, the distinction is ambiguous. In the non linear regime of forward cascade, the reference to KH is probably more justified.

The understanding of residual stress in term of initial eddy tilt is more delicate in case of broadband turbulent systems involving a superposition of eddy chains. At the simplest understanding level, Reynolds stresses would add. The negative viscosity component arises from an intrinsic symmetry breaking property of the system with shear flow [29] and naturally eddies immersed within the same background sheared flow will all contribute to the net overall stress. Similarly, residual stresses of such a set of eddies would also add together. Then, a broad distribution of eddies with random initial tilts is likely to cancel the residual stress term after summation, in the case there are no general reasons to invoke another breaking of symmetry in the turbulence phase space. Recently, it was proposed that magnetic shear, under specific circumstances, can provide such additional breaking [18]. We examine this effect in more detail next.

IV. REYNOLDS STRESS PROVIDED BY MAGNETIC SHEAR

The magnetic shear induces a continuous stretching of flux tubes along the parallel direction. Since transport anisotropy in tokamaks forces transverse perturbations to be almost uniform along field lines ($k_z \approx 0$), their transverse (x, y) cross sections are non uniform along flux surfaces, as illustrated in Fig.3. This property is well known from numerical simulations (See [30] or other illustrations in [31–33]). Existing observations from C-mod [34], Tore-Supra [35], EAST [36] or TJ-K [37] agrees with the picture shown in Fig.3. From the above discussion, such local tilt induces a local Reynolds stress that varies with the poloidal position since the magnetic shear induced tilting is not constant along the poloidal chain axis (y or θ). Given a reference poloidal position θ_0 on a flux surface, a flux tube cross section of radial wave number $k_x(\theta_0)$ at this reference location is evolving in the parallel/poloidal direction following the relation [18]:

$$k_x(\theta) = k_x(\theta_0) + (\theta - \theta_0) k_y \hat{s} \tag{7}$$

where $\hat{s} = \frac{r}{q}\partial_r q$ is the magnetic shear and k_y is the poloidal wave vector, both assumed uniform along θ. This relation holds for one particular chain of coherent eddies. For a given reference location θ_0, a superposition of modes with random reference wave vector $k_{x,0}$ will not impact the contribution of magnetic shear to the local effective tilt. On the other hand, a superposition of modes having random reference positions will cancel this contribution. That said, at the edge of L-mode plasmas, transport is believed to have a ballooning nature ([39] for modeling and [40–

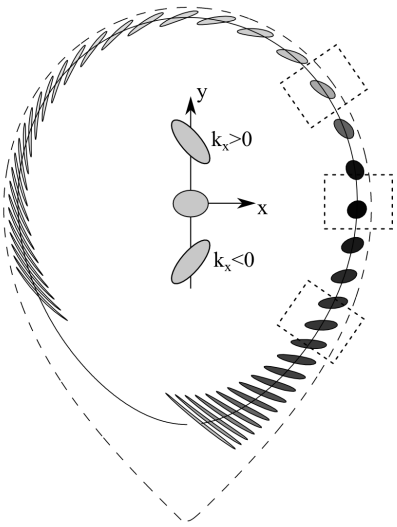

FIG. 3. Flux tube geometry on a magnetic equilibrium as used in [38]. The tube is initiated by a circular cross section at the outboard midplane ($\theta_0 = 0$). The cross section is tilted in the local coordinate system, depending on the poloidal position.

43] for experimental works). Thus, modes are essentially excited at the outboard midplane or around ($\theta_0 \approx 0$), so that in average, eddies have a local effective tilt influenced by the magnetic shear [30, 34–36]. Deviation from the peaking position $\theta_0 = 0$ generally exist, principally due to shear flows [18, 31], but we further neglect this effect by assuming the system is in the weak shear regime. Consequently, Eq.7 reduces to $k_x(\theta) = k_y \theta \hat{s}$ after summation over a spectrum of ballooning modes having random $k_{x,0}$. Effect of negative viscosity should also be added to the tilt, so that $k_x(\theta) = -k_y \sigma_S \tau + k_y \theta \hat{s}$. The Reynolds stress associated to this mode structure takes the form (see Eq.6):

$$\left\langle \tilde{v}_r \tilde{v}_y \right\rangle_t (\theta) \approx \underbrace{\left\langle v_r^2 \right\rangle (\theta) \tau \sigma_S}_{\Pi_V(\theta)} - \underbrace{\theta \hat{s} \left\langle v_r^2 \right\rangle (\theta)}_{\Pi_{\hat{s}}(\theta)} \tag{8}$$

where we identify the negative viscosity stress Π_V and the magnetic shear induced stress $\Pi_{\hat{s}}$. We keep explicit a poloidal dependence of the ballooning fluctuation amplitude $\langle v_r^2 \rangle (\theta)$. In the equation describing the large scale transverse flow V_E evolution, the turbulent source term takes the form of a poloidal or flux surface average of the Reynolds stress [4]. From Eq.8, we readily see that that $\Pi_{\hat{s}}$ is generally antisymmetric along θ: contributions above and below the midplane tend to compensate. The poloidal residual $\langle \Pi_{\hat{s}} \rangle = \langle \theta \hat{s} \langle v_r^2 \rangle (\theta) \rangle_\theta$, is finite only for an up/down asymmetric turbulence activity. Toward the plasma center, magnetic flux surfaces are symmetric and turbulence activity is likely to respect this symmetry: there is no or very little magnetic shear

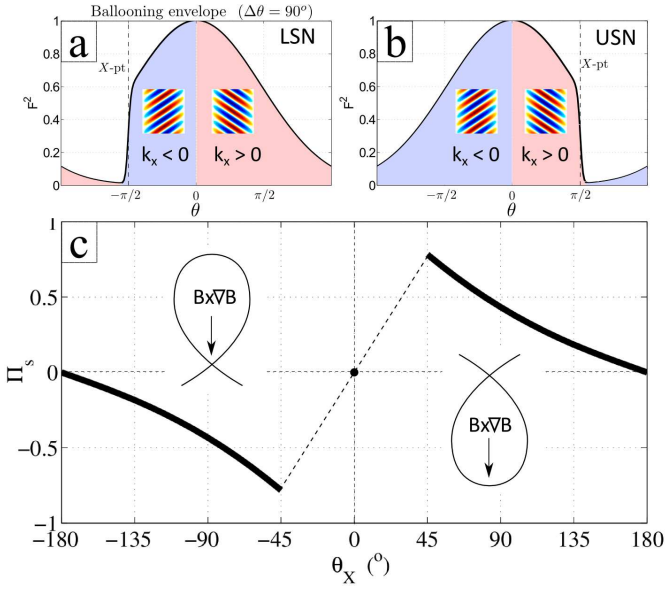

FIG. 4. **a)** and **b)** Poloidal envelope of ballooning modes on flux surfaces affected by X-point resistivity, for lower single null and upper single null geometries. Sections of positive and negative tilting are illustrated. **c)** Amplitude of the poloidal average of the magnetic shear induced Reynolds stress $\langle \theta \hat{s} \langle v_r^2 \rangle \rangle_\theta / \langle \langle v_r^2 \rangle \rangle_\theta$, as a function of the X-point position, for a magnetic configuration such that the ion diamagnetic direction is toward the bottom.

induced stress in the core region. As explained in [18], the situation changes toward the boundary of the confined region. In the vicinity of the separatrix, X-point resistivity [44] damps the parallel extent of the ballooning envelope, inducing an asymmetry with respect to the plasma crown where the mode is free to extend along field lines. This asymmetry naturally exists in the scrape-of-layer of limited or X-point plasmas, where it also induces parallel flows based on similar asymmetry arguments [40, 41, 43]. The poloidal symmetry breaking of ballooning envelopes therefore takes place at the boundary of both limiter and X-point plasmas, justified by either X-point resistivity or end-plates boundary arguments. As illustrated in Fig.4a&b, this poloidal truncation of the ballooning envelope creates an unbalance between positive tilt and negative tilt contributions to the total stress. For a geometry with an X-point or limiter toward the ion diamagnetic drift direction (in our sign convention $\theta_X < 0$), the negative tilt contribution dominates. It obviously reverses if the X-point position is switched. Also, moving the X-point closer to the midplane reduces the contribution of the tilt between the midplane and the X-point and increases the symmetry breaking. At the contrary moving the X-point toward the inboard midplane tends to balance positive and negative tilt contributions. These variations are shown in Fig.4c, where is reported

the stress amplitude function of the X-point or limiter poloidal position. Note that in its principle, this poloidal symmetry breaking argument was already invoked by Camenen et al. [17] for its contribution to the drive of parallel rotation. In the present work, we show that it is also capable of driving transverse rotation.

An ordering is necessary to assess the importance of this term at the edge, compared to the negative viscosity. As shown in Fig.4, the magnetic shear residual stress is a consequent fraction of the radial drift energy of the turbulence $\langle \Pi_{\hat{s}} \rangle_\theta = \alpha \langle \langle v_r^2 \rangle \rangle_\theta$ with $\alpha \approx 0.5$ for a ballooning envelope of poloidal opening $\Delta\theta = 90^o$. In the limit of *flute* ballooning modes ($\Delta\theta \rightarrow +\infty$), the stress is even stronger $\alpha \approx 3$ in LSN configurations. In the negative viscosity expression (Eq.8), the same coefficient is equal to $\alpha = \tau\sigma_S$ which is the product of the eddy residence or life time with the flow shear. Now considering that the tilting instability depletes eddies over the inverse of the shearing rate [22], which is also the ordering of the eddy life time found in TEXTOR across the edge shearing region [45], this parameter is found close to unity. Thus, both negative viscosity and magnetic shear stress are of equal importance in the edge momentum balance regarding the impact of turbulence.

V. IMPACT ON EDGE RADIAL ELECTRIC FIELD IN TOKAMAKS

In L-mode tokamak plasmas, the core radial electric field is generally inward from the neoclassical ion force balance [46], and outward in the scrape off layer due to sheath boundary conditions [47]. Thus, by continuity, the flow shear is generally negative just inside the separatrix. Besides, as explained above, an X-point located in the direction of the ion diamagnetic drift imposes a positive radial wave vector $k_x > 0$ and a negative magnetic shear residual stress (Fig.4) at the plasma boundary. With a negative shear σ_S, the system is thus in the favorable tilt regime $k_x\sigma_S < 0$, meaning that the magnetic shear stress adds to the negative viscosity. On the other hand, for an X-point located away from the ion diamagnetic drift direction, the magnetic shear stress reverses and the system is in the unfavorable tilt regime $k_x\sigma_S > 0$: the magnetic shear stress competes with the negative viscosity. The favorable tilt regime is likely to produce an equilibrium shear flow of stronger amplitude than the unfavorable regime since the shear drive is stronger.
These favorable (unfavorable) tilt regimes also correspond to plasma geometries defined as favorable (unfavorable) with respect to the amount of input power required to trigger the H-mode [48]. Several observations from different tokamaks pointed out that the flow shear measured at

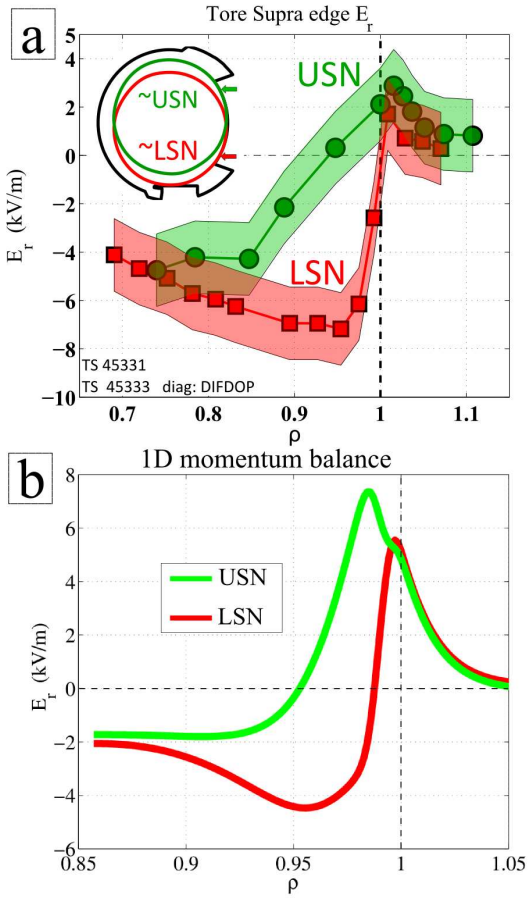

FIG. 5. **a)** Radial electric field profile measured with Doppler back scattering at the edge of Tore Supra ohmic plasmas. The plasma is in contact with toroidally quasi-symmetric limiters, either below or above the midplane. These configurations are analogous to lower SN and upper SN. **b)** Equilibrium radial electric field calculated with the 1D momentum balance Eq.9 for lower SN and upper SN configurations.

the boundary of L-mode plasmas was indeed weaker for unfavorable geometries than for favorable geometries [19, 20].

We quantify these effects as follows. In [18], a transverse ion momentum balance was proposed with the inclusion of the magnetic shear stress:

$$\partial_t V_E + \frac{1}{n}\partial_r \left[n \left(\Pi_{\hat{s}} + \Pi_V \right) \right] = - \left[\nu_{cx} - \chi_\perp \partial_r^2 \right] \left(V_E + V_i^* \right) \tag{9}$$

where the RHS term contains a linear damping - charge exchange with neutrals for instance- and a diffusion term in the range of gyro-Bohm scalings. Following the weak shear approximation, kinetic profiles are considered frozen, especially the pressure and so the diamagnetic velocity profile V_i^*. Not shown in Eq.9 is also a damping term effective only in the SOL which forces the radial electric

field to be $E_r = -3\partial_r T_e$. With generic parameter values as used in [18], equilibrium solutions of Eq.9 can be calculated for different plasma geometries illustrated in Fig.5b. For a lower single null (LSN) configuration (favorable geometry), the radial electric field is more negative just inside the separatrix than for the upper single null. It is a consequence of fixed electric field condition in the SOL and stronger gradient in LSN configuration provided by the residual stress. Profiles shown in Fig.5b are built with parameters typical of L-mode plasma discharges, and thus should give a correct ordering of the change of edge radial electric field between LSN and USN configurations in L-mode plasmas. A comparison with Tore Supra data is presented in Fig.5a. Plasmas are circular, ohmically heated and limited on the low field side by a quasi-toroidally symmetric limiter. By moving the plasma up and down, the contact point with this limiter is rolled from $\theta_X \approx -35^o$ below the midplane (equivalent to LSN) to $\theta_X \approx +35^o$ above the midplane (equivalent to USN). The change in edge radial electric field measured by Doppler back-scattering reflectometry [21] is as follow: it is more negative just inside the last closed flux surface for LSN than for USN configurations, quite similar in shape and amplitude to what is calculated by the model. It is true that Tore Supra limiter plasmas do not have an X-point and thus X-point resistivity does not exist in the confined region. That said it still exists in the SOL and across the separatrix, and limiter configurations induce a strong and local ionization/radiation volume in the confined region just ahead of the contact point [43], which could play a similar role as the X-point resistivity. Profiles shown here for Tore Supra plasmas are very similar to LSN and USN profiles measured at the edge of ASDEX L-mode plasmas (see Fig.4 in ref.[20]). Finally, it is worth mentioning that for the discharges associated with these E_r profiles, the global momentum is different, although we previously pointed out that tilt stresses only re-organize the existing momentum. This non conservation is due to the scrape-off layer volume which acts as a source of momentum: Reynolds stress at the separatrix can transport momentum to the open field line region where it is dissipated by parallel losses to the end-plates. This physics is beyond the scope of the model introduced here, but could be an important mechanism to study in future work.

VI. CONCLUSION

The dynamical interaction between potential eddies and shear flow can be approximated with a simplified model of tilted eddies, which contains the minimum physics to describe different phenomena. The tilting instability occurs when eddies are favorably tilted with respect to the flow shear. It induces a growth of the shear while the eddies get stretched and depleted. The shear

flow apparently breaks apart the eddies due a local transfer of energy. The non linear dynamics evolves into forward cascade in radial modulation, understood as a succession of Kelvin-Helmholtz and tilting processes. The KH happens within the depleted eddies and forces the flow to generate smaller structures, which will become tilting unstable after a finite period of time. On the initial modulation scale, the tilting instability dominates and we speak of negative viscosity. In fact the flow shear gains energy out of the eddies but the KH induces a cascade to smaller scales where a fraction of the initial energy gets eventually dissipated. The initial tilting instability can however be influenced by the existence of an intrinsic eddy tilt, which also corresponds to a residual stress. An intrinsic tilt aligned with (opposite to) the shear is defined as favorable (unfavorable) because it adds to (compensate) the negative viscosity. In general, the system has to exhibit a symmetry breaking so that eddies exhibit systematically the same intrinsic tilt. In tokamak geometry, such tilt can be provided by the differential helicity of the field lines, which creates an up/down asymmetric tilt on ballooning modes. The system also needs a spatial asymmetry of the ballooning turbulence activity, so that a particular sign of the magnetic shear tilt dominates on a flux surface. At the edge boundary, the X-point or limiter region provides this poloidal symmetry breaking. In the weak shear regime, the residual tilt is relatively strong compared to negative viscosity. Moreover, its sign and amplitude are function of the X-point or limiter location: an X-point position is then said favorable when the magnetic shear tilt is favorably oriented with respect to the local flow shear, and so adds to the negative viscosity to enforce the local shear. Just inside the separatrix where the magnetic shear tilt is finite, the flow shear is generally such that the favorable geometry corresponds to X-points positioned in the direction of the ion diamagnetic drift. It is indeed a plasma configuration for which the strongest shear is measured in L-mode, and this model of stress is able to explain the change of flow profile from a lower single null to an upper single null geometry. Future investigations should focus on a more realistic description of developed ballooning turbulence with shear flows at the edge of tokamaks plasmas, including realistic X-point geometry.

ACKNOWLEDGMENT

This work, supported by the European Communities under the contract of association between EURATOM and Commissariat á l Energie Atomique et aux energies alternatives, was carried out within the framework of the European Fusion Development Agreement. The views and opinions

expressed herein do not necessarily reflect those of the European Commission.

---

[1] D. J. Ward and A. Bondeson. *Physics of Plasmas*, 2(5):1570–1580, 1995.

[2] Keith H. Burrell. *Physics of Plasmas*, 6(12):4418–4435, 1999.

[3] F Wagner. *Plasma Physics and Controlled Fusion*, 49(12B):B1, 2007.

[4] P H Diamond, S-I Itoh, K Itoh, and T S Hahm. *Plasma Physics and Controlled Fusion*, 47(5):R35, 2005.

[5] K. H. Burrell. *Physics of Plasmas*, 4(5):1499–1518, 1997.

[6] H. Biglari, P.H. Diamond, and P.W. Terry. *Phys. Fluids B*, 2, 1990.

[7] P. H. Diamond and Y.-B. Kim. *Physics of Fluids B: Plasma Physics*, 3(7):1626, 1991.

[8] J. F. Drake, J. M. Finn, P. Guzdar, V. Shapiro, V. Shevchenko, F. Waelbroeck, A. B. Hassam, C. S. Liu, and R. Sagdeev. *Physics of Fluids B: Plasma Physics*, 4(3):488, 1992.

[9] M. N. Rosenbluth and V. D. Shapiro. *Physics of Plasmas*, 1(2):222–224, 1994.

[10] P. N. Guzdar, J. F. Drake, D. McCarthy, A. B. Hassam, and C. S. Liu. *Physics of Fluids B: Plasma Physics*, 5(10):3712–3727, 1993.

[11] P. Manz, M. Ramisch, and U. Stroth. *Phys. Rev. Lett.*, 103:165004, 2009.

[12] M. Xu, G. R. Tynan, P. H. Diamond, C. Holland, J. H. Yu, and Z. Yan. *Phys. Rev. Lett.*, 107:055003, Jul 2011.

[13] D. L. Jassby. *Physics of Fluids*, 15(9):1590–1604, 1972.

[14] T.C. Hender, J.C Wesley, J. Bialek, A. Bondeson, A.H. Boozer, R.J. Buttery, A. Garofalo, T.P Goodman, R.S. Granetz, Y. Gribov, O. Gruber, M. Gryaznevich, G. Giruzzi, S. Gnter, N. Hayashi, P. Helander, C.C. Hegna, D.F. Howell, D.A. Humphreys, G.T.A. Huysmans, A.W. Hyatt, A. Isayama, S.C. Jardin, Y. Kawano, A. Kellman, C. Kessel, H.R. Koslowski, R.J. La Haye, E. Lazzaro, Y.Q. Liu, V. Lukash, J. Manickam, S. Medvedev, V. Mertens, S.V. Mirnov, Y. Nakamura, G. Navratil, M. Okabayashi, T. Ozeki, R. Paccagnella, G. Pautasso, F. Porcelli, V.D. Pustovitov, V. Riccardo, M. Sato, O. Sauter, M.J. Schaffer, M. Shimada, P. Sonato, E.J. Strait, M. Sugihara, M. Takechi, A.D. Turnbull, E. Westerhof, D.G. Whyte, R. Yoshino, H. Zohm, Disruption the ITPA MHD, and Magnetic Control Topical Group. *Nuclear Fusion*, 47(6):S128, 2007.

[15] T. E. Stringer. *Phys. Rev. Lett.*, 22:770–774, 1969.

[16] A. B. Hassam, Jr. T. M. Antonsen, J. F. Drake, P. N. Guzdar, C. S. Liu, D. R. McCarthy, and F. L. Waelbroeck. *Physics of Fluids B: Plasma Physics*, 5(7):2519–2524, 1993.

[17] Y. Camenen, A. G. Peeters, C. Angioni, F. J. Casson, W. A. Hornsby, A. P. Snodin, and D. Strintzi. *Phys. Rev. Lett.*, 102:125001, 2009.

[18] N. Fedorczak, P.H. Diamond, G. Tynan, and P. Manz. *Nuclear Fusion*, 52(10):103013, 2012.

[19] T N Carlstrom, R J Groebner, C Fenzi, G R McKee, R A Moyer, and T L Rhodes. *Plasma Physics and Controlled Fusion*, 44(5A):A333, 2002.

[20] H. Meyer, P.G. Carolan, G.D. Conway, G. Cunningham, L.D. Horton, A. Kirk, R. Maingi, F. Ryter, S. Saarelma, J. Schirmer, W. Suttrop, H.R. Wilson, the MAST, ASDEX Upgrade, and NSTX teams. *Nuclear Fusion*, 46(1):64, 2006.

[21] P. Hennequin, C. Honor, A. Truc, A. Quéméneur, C. Fenzi-Bonizec, C. Bourdelle, X. Garbet, G.T. Hoang, and the Tore Supra team. *Nuclear Fusion*, 46(9):S771, 2006.

[22] N. Fedorczak, P. Manz, S.C. Thakur, M. Xu, and G.R. Tynan. *Plasma Physics and Controlled Fusion*, 55(2):025011, 2013.

[23] Y. Sarazin and Ph. Ghendrih. *Physics of Plasmas*, 5(12):4214–4228, 1998.

[24] P. N. Guzdar. *Physics of Plasmas*, 2(11):4174–4176, 1995.

[25] V S Mikhailenko, V V Mikhailenko, and K N Stepanov. *Plasma Physics and Controlled Fusion*, 52(5):055007, 2010.

[26] R. H. Kraichnan. *Physics of Fluids*, 10(7):1417–1423, 1967.

[27] Ö. D. Gürcan, P. H. Diamond, T. S. Hahm, and R. Singh. *Physics of Plasmas*, 14(4):042306, 2007.

[28] E-J. Kim and P. H. Diamond. *Phys. Rev. Lett.*, 91:075001, 2003.

[29] P.H. Diamond, C.J. McDevitt, .D. Grcan, T.S. Hahm, W.X. Wang, E.S. Yoon, I. Holod, Z. Lin, V. Naulin, and R. Singh. *Nuclear Fusion*, 49(4):045002, 2009.

[30] P. Beyer, S. Benkadda, X. Garbet, and P. H. Diamond. *Phys. Rev. Lett.*, 85:4892, 2000.

[31] J. Y. Kim, Y. Kishimoto, M. Wakatani, and T. Tajima. *Physics of Plasmas*, 3(10):3689–3695, 1996.

[32] F. Jenko, D. Told, P. Xanthopoulos, F. Merz, and L. D. Horton. *Physics of Plasmas*, 16(5):055901, 2009.

[33] Y. Camenen, Y. Idomura, S. Jolliet, and A.G. Peeters. *Nuclear Fusion*, 51(7):073039, 2011.

[34] J.L. Terry, S.J. Zweben, M.V. Umansky, I. Cziegler, O. Grulke, B. LaBombard, and D.P. Stotler. *Journal of Nuclear Materials*, 390(0):339 – 342, 2009.

[35] N. Fedorczak, J. P. Gunn, J.-Y. Pascal, Ph. Ghendrih, G. van Oost, P. Monier-Garbet, and G. R. Tynan. *Physics of Plasmas*, 19(7):072314, 2012.

[36] N. Fedorczak, P. Manz, S. C. Thakur, M. Xu, G. R. Tynan, G. S. Xu, and S. C. Liu. *Physics of Plasmas*, 19(12):122302, 2012.

[37] G Birkenmeier, M Ramisch, G Fuchert, A Köhn, B Nold, and U Stroth. *Plasma Physics and Controlled Fusion*, 55(1):015003, 2013.

[38] A. Loarte and P.J. Harbour. *Nuclear Fusion*, 32(4):681, 1992.

[39] C Bourdelle, X Garbet, R Singh, and L Schmitz. *Plasma Physics and Controlled Fusion*, 54(11):115003, 2012.

[40] B. LaBombard, J.E. Rice, A.E. Hubbard, J.W. Hughes, M. Greenwald, J. Irby, Y. Lin, B. Lipschultz, E.S. Marmar, C.S. Pitcher, N. Smick, S.M. Wolfe, S.J. Wukitch, and the Alcator Group. *Nuclear Fusion*, 44(10):1047, 2004.

[41] J.P. Gunn, C. Boucher, M. Dionne, I. ÄZuran, V. Fuchs, T. Loarer, I. Nanobashvili, R. Pánek, J.-Y. Pascal, F. Saint-Laurent, J. Stöckel, T. Van Rompuy, R. Zagórski, J. Admek, J. Bucalossi, R. Dejarnac, P. Devynck, P. Hertout, M. Hron, G. Lebrun, P. Moreau, F. Rimini, A. Sarkissian, and G. Van Oost. *Journal of Nuclear Materials*, 363-365(0):484, 2007.

[42] P. Manz, M. Ramisch, and U. Stroth. *Physics of Plasmas*, 16(4):042309, 2009.

[43] N. Fedorczak, J. P. Gunn, J.-Y. Pascal, Ph. Ghendrih, Y. Marandet, and P. Monier-Garbet. *Physics of Plasmas*, 19(7):072313, 2012.

[44] J. R. Myra, D. A. D'Ippolito, X. Q. Xu, and R. H. Cohen. *Physics of Plasmas*, 7(6):2290–2293, 2000.

[45] I. Shesterikov, Y. Xu, C. Hidalgo, M. Berte, P. Dumortier, M. Van Schoor, M. Vergote, and G. Van Oost. *Nuclear Fusion*, 52(4):042004, 2012.

[46] E. Trier, L.-G. Eriksson, P. Hennequin, C. Fenzi, C. Bourdelle, G. Falchetto, X. Garbet, T. Aniel, F. Clairet, and R. Sabot. *Nucl. Fusion*, 48(9):092001, 2008.

[47] A.V. Chankin, D.P. Coster, N. Asakura, X. Bonnin, G.D. Conway, G. Corrigan, S.K. Erents, W. Fundamenski, J. Horacek, A. Kallenbach, M. Kaufmann, C. Konz, K. Lackner, H.W. Müller, J. Neuhauser, R.A. Pitts, and M. Wischmeier. *Nuclear Fusion*, 47(5):479, 2007.

[48] G.R. McKee, P. Gohil, D.J. Schlossberg, J.A. Boedo, K.H. Burrell, J.S. deGrassie, R.J. Groebner, R.A. Moyer, C.C. Petty, T.L. Rhodes, L. Schmitz, M.W. Shafer, W.M. Solomon, M. Umansky, G. Wang, A.E. White, and X. Xu. *Nuclear Fusion*, 49(11):115016, 2009.